EVOLUTION OF THE REGIONAL CODA METHODOLOGY

Kevin M. Mayeda[1], W. Scott Phillips[2], Luca Malagnini[3], and Douglas S. Dreger[4]

Lawrence Livermore National Laboratory[1], Los Alamos National Laboratory[2],
Istituto Nazionale di Geofisica e Vulcanolgia[3], and University of California at Berkeley[4]

Sponsored by National Nuclear Security Administration
Office of Nonproliferation Research and Engineering
Office of Defense Nuclear Nonproliferation

Contract No. W-7405-ENG-48, W-7405-ENG-36

ABSTRACT

For the past decade, Lawrence Livermore National Laboratory (LLNL) and Los Alamos National Laboratory (LANL), have been developing and testing a stable, regional coda magnitude methodology for the determination of magnitude and yield. The motivation behind this research was to take advantage of the averaging nature of coda waves in support of monitoring small seismic events from a sparse regional seismic network (*e.g.*, International Monitoring System (IMS) network). The methodology as described in Mayeda et al., (2003) has been successfully applied in a variety of tectonic settings where the assumption of a one-dimensional (1-D), radially symmetric path correction was sufficient. In general, this resulted in interstation amplitude scatter that was 3 to 4 times smaller than the traditional approach using direct *S*, *Lg,* and surface waves ($0.02 < f < 8.0$-Hz). However, in more laterally complex regions there is a need to extend this approach to account for smaller-scale 2-D variations in structure, especially at frequencies above ~1 Hz. Recently, Phillips et al., (2003) have applied a 2-D approach to data in central Asia by assuming that the coda-envelope amplitude could be idealized as if it were a direct wave. They performed a tomography to invert for *Q* along the path and through the choice of damping parameter and geometrical spreading, they in effect distributed the attenuation over an area, not unlike what has been previously assumed in the single-scattering model of Aki (1969) where the attenuation is attributed to an ellipsoidal volume.

As a test of the two methods, we chose over 100 well-located earthquakes ($3.5 < Mw < 6.5$) distributed throughout the northern California region recorded on high-quality broadband stations of the Berkeley Digital Seismic Network (BDSN). The complicated tectonics of the region coupled with this high-quality data, provide for an ideal situation to test the two approaches. We found that source spectra derived from the 2-D approach were essentially identical to those from the 1-D approach for frequencies less than ~0.7 Hz; however, for the high frequencies ($0.7 < f < 8.0$-Hz), the 2-D approach resulted in interstation scatter that was generally 30% smaller. Since our main objective is to improve moment-magnitude estimation for small regional events, the 30% improvement is significant in helping to meet the United States (U.S.) monitoring goals.

OBJECTIVES

The purpose of this study is several fold. First and foremost, the accurate determination of M_o, E_R, and derived stress drop is important in understanding the scaling of earthquakes, which is a key component in the estimation of seismic hazards in a region. Second, magnitudes that are presently determined for events in Northern California come in a variety of forms, which include duration magnitudes (M_D), local magnitudes (M_L), and moment magnitude (M_w) for events $M_L > \sim 3.5$. By using the method of Mayeda et al., (2003) a new M_w(coda) scale was developed that is continuously defined for all earthquakes between $\sim 1 < M_w < 7+$. Over the past several years, the empirically derived coda methodology has provided unprecedented stability in source-spectral estimates for earthquakes and underground nuclear explosions (UNE's) recorded at local and regional distances. For example, the coda-derived source spectra have provided the most stable estimates of magnitude and yield for Nevada Test Site (NTS) explosions (*e.g.*, single-station F-values are less than 1.7) and were successfully transported to foreign test sites such as Lop Nor, Novaya Zemlya, and Semipalitinsk. More recently, the methodology has been successfully applied to earthquakes recorded by small local networks in the Eastern Alps (Malagnini et al., 2004), Western Alps (Morasca et al., 2004), as well as the Dead Sea rift in the Middle East (Mayeda et al., 2003). For the broader regions, Eken et al., (2004) found that the standard 1-D path correction of Mayeda et al., (2003) for the region in and around Turkey was valid between 0.02 and 2.0 Hz, but not for higher frequencies. The success of the coda methodology is commonly believed to come from the volume averaging of the coda waves that sample the entire focal sphere and renders them virtually insensitive to any source radiation pattern effect and path heterogeneity (e.g., Aki, 1969; Aki and Chouet, 1975; Rautian and Khalturin, 1978). Both the observational and theoretical studies of the past several decades are reviewed thoroughly by Sato and Fehler (1998). In the current study, we compare performance between coda and direct waves using both 1-D and 2-D formulations for the path effect using the same events and stations. Our final results (source spectra) are validated against ground-truth moment estimates as well as network-averaged direct wave spectra corrected for path and site effects using both 1-D and 2-D path corrections.

RESEARCH ACCOMPLISHED

Our findings are as follows: (1) 2-D path corrections for the direct waves significantly reduces the scatter over 1-D corrections; however, interstation scatter remains large, ranging between ~0.18 and 0.3 for $0.1 < f < 8.0$-Hz; (2) 1-D coda path corrections result in scatter that is roughly 50% smaller than the 2-D direct-wave results; (3) 2-D coda path corrections result in data scatter that is ~10 to 30% smaller than the 1-D coda results.

Geologic Setting and Data

In the simplest terms, Northern California has a pronounced thickening of the crust from west to east, from 25 km on average in the San Francisco region to more than 40 km beneath the Sierra Nevada. Average crustal velocity and near-surface velocity gradients differ significantly between the Coast Ranges and the Sierra Nevada (Dreger and Romanowicz, 1994). The San Joaquin Valley, a sedimentary basin with thicknesses as great as 4 km, produces complicated surface waves. The northern part of the state is influenced by the southern reaches of the Cascade volcanic arc. Observed broadband waveforms (e.g., Dreger and Romanowicz, 1994, and surface wave-group velocity variations (Pasyanos et al., 1996) reflect the geologic complexity.

The U.C. Berkeley moment tensor catalog and broadband waveform dataset is ideal for testing and applying the regional coda envelope method because of the high level of ground truth. Seismic moment tensors have been routinely computed from both complete three-component waveforms, surface wave amplitude, and phase spectra since 1993 (Romanowicz et al., 1993; Pasyanos et al., 1996). These codes are fully automated at the Berkeley Seismological Laboratory (BSL) and have been applied successfully in other regions of the world (e.g., Fukuyama et al., 1998; Fukuyama and Dreger, 2000; Örgülü and Aktar, 2001), and has been tested for near-realtime, continuous operation (Tajima et al., 2002). The complete waveform method has been recently expanded to allow for the investigation of full moment tensors (Dreger et al., 2000), and a double-couple plus isotropic model (e.g., Dreger and Woods, 2002), which is useful for studying volcanic and geothermal-related events as well as man-made explosions. The seismic moment tensors are routinely determined for events with $M_L > \sim 3.4$ ranging in magnitude from M_w 3.5 to 7.0. Currently, the broadband BDSN has expanded to 20 stations providing excellent regional coverage of the distributed seismicity of northern and central California (Figure 1).

We selected 144 events distributed throughout northern California of which approximately 100 of these had moment tensor solutions derived from multiple station inversions ranging between $3.5 < M_w < 6.5$ (see Figure 1). In total, we calibrated 16 BDSN broadband stations in this study, but as will be shown later, we used a subset of these stations to derive the calibration parameters. The point of this was to show the robustness of the calibration procedure and the ease to which calibration parameters could be applied to new stations.

Coda Method

The 1-D coda methodology is described in detail by Mayeda et al., (2003) so we give only a short, qualitative review here. In contrast to direct-wave measurements, the coda method is based upon narrowband amplitude measurements taken simultaneously from the envelope ranging from several tens of seconds up to hours depending on the frequency band and event magnitude (e.g., Mayeda and Walter, 1996). In the simplest terms, a coda envelope amplitude measurement significantly reduces the variance associated with 3-D path heterogeneity, random interference, and source heterogeneity, which strongly affect the direct waves. The codas we use are composed of local *S*-waves, regional L_g, and long-period surface waves. In spite of these various wave types, which travel at different velocities and sample different parts of the focal sphere, our empirically derived corrections produce very stable *S*-wave source spectra from as few as one station.

The coda envelopes for each frequency band can be idealized with the following equation,

$$\mathrm{A_c}(f, t, r) = W_o(f) \cdot S(f) \cdot T(f) \cdot P(r, f) \cdot H(t - t_s) \cdot (t - t_s)^{-\gamma(r)} \exp\left[-b(r) \cdot (t - t_s)\right] , \quad (1)$$

where f is the center frequency, r is the epicentral distance in kilometers, t is the time in seconds from the origin time, t_s is the *S*-wave travel time in seconds, W_o represents the *S*-wave source, S is the site effect, T represents the *S*-to-coda transfer function effect, P includes the distant-dependent effects of geometrical spreading and attenuation, H is the Heaviside step function, $\gamma(r)$ and $b(r)$ are the distance-dependent coda shape factors that controls the coda envelope shape. For simplicity, we have set $\gamma = 0.2$ noting that this parameter only controls the early part of the coda immediately following the direct arrival which is more influenced by source radiation pattern. Because we are fitting the coda over large amounts of time, the exponential term $b(r)$ is the most important parameter because it controls the majority of the coda envelope shape. However, for the purpose of generating synthetics we set *W, S, T,* and *P* to unity. Following the methodology outlined in Mayeda et al., (2003), the coda shape parameters and velocity of the peak S/L_g-wave arrival were fit as a function of distance using the form of a hyperbola.

1-D Coda Path Corrections

In the following, we briefly review how we derived 1-D path corrections. For each narrowband envelope in our dataset, raw coda amplitudes were determined by generating synthetics at the appropriate distance and using a source of unity then DC shifting using an L-1 norm to fit the observed envelope. The amount of the DC shift is the nondimensional raw coda amplitude. Next, we use the following empirical equation for the coda path correction of Mayeda et al., (2003).

$$P(r, f) = \left[1 + \left(\frac{r}{p_2}\right)^{p_1}\right]^{-1} \quad (2)$$

We used common recordings using 6 station pairs and then grid-searched over p_1 and p_2 and tabulated the interstation scatter for each frequency band. The 6 pairs were chosen such that there was good geographic sampling and are shown in Figure 1. The choice of a frequency-dependent path correction for the entire region was based upon the path parameters p_1 and p_2 that gave the lowest average interstation standard deviation between our six station pairs. To test the robustness of the method, we compared path parameters using completely different station combinations, and the results were virtually unchanged. With path parameters determined, we can transform our synthetics to path-corrected envelopes. Finally, we applied the path corrections to all the data, including the other 10 stations that were not part of the path-calibration procedure. In the following, we consider the direct waves so that we can compare directly, one-to-one, the coda results.

1-D Direct Waves Path Corrections

For every coda amplitude that was measured, we also measured the corresponding peak amplitude of the direct wave (e.g., *S*, L_g or surface waves). As done previously with the coda, we applied a grid search using the same events and stations to estimate the best value of *Q* using the formulation of Street *et al*., (1975), where the direct wave amplitude at distance *r* and frequency *f* is,

if $r < r_c$

$$A(r,f) = A_0 \cdot S(f) \cdot \frac{1}{r} \cdot e^{-\left[\frac{\pi f}{\beta Q_\beta}\right]}$$

and if $r \geq r_c$

$$A(r,f) = A_0 \cdot S(f) \cdot \frac{1}{r_c} \cdot \left(\frac{r_c}{r}\right)^{\gamma} \cdot e^{-\left[\frac{\pi f}{\beta Q_\beta}\right]} \quad (3)$$

where A_0 is the source term, *S* is the site effect, r_c is the critical distance (fixed at 100 km), γ is the spreading coefficient (set to 0.5), β is the *S*-wave velocity, and Q_β is the *S*-wave quality factor. We chose this formulation because it accounts for both local *S*-wave geometrical spreading, ($1/r$) at distances less than r_c, and transitions smoothly to L_g spreading, ($1/r^{0.5}$) when *r* is greater than r_c. We then solved for the best value of *Q* that minimized the scatter between the same six station pairs that were used for the coda path corrections. The averaged *Q* follows the form, $Q(f) = 90 f^{0.64}$ for frequencies between 0.3 and 8.0 Hz. As found with the coda, a different choice of station pairs had little to no effect on the resulting *Q* values.

2-D Direct and Coda Path Corrections

For both the direct waves and coda waves, we assumed the same formulation as that shown in Equation 3. However, for the case of the coda, we set the geometrical spreading parameter to 0 and just inverted for $1/Q$ only. The inversion we chose is a least-squares algorithm (LSQR) that inverts for $1/Q$ using a grid size of 0.1 degree. As done previously, we performed a tomography to invert for $1/Q$ along the path and through the choice of damping parameter and geometrical spreading, and in effect distributed the attenuation over an area, not unlike what has been previously assumed in the single-scattering model of Aki (1969) where the attenuation is attributed to an ellipsoidal volume. Figure 2a and 2b show maps of *Q* for both direct waves and coda for the case of 3.0–4.0 Hz. Notice that the two figures are remarkably similar even though the wave types are completely different. In general, comparisons with other frequency bands were similar, all showing higher *Q* in the Sierra Nevada and lower *Q* in the Cascade ranges extending down into the Franciscan formation, including the Geysers geothermal field.

Comparison Between Coda and Direct Waves

For frequencies ranging between 0.1 and 8.0 Hz, Figure 3 summarizes the average interstation standard deviation derived from up to 45 station pairs for distance-corrected coda and direct waves. In general, the average interstation standard deviation for all measures (e.g., 1-D *S*-wave, 2-D *S*-wave, 1-D coda, 2-D coda) increases with increasing frequency. First, we observe that the 2-D path corrections for the direct waves significantly reduce the scatter over 1-D corrections; however, the interstation scatter remains large, ranging between ~0.18 and 0.3. Second, the 1-D coda path corrections result in scatter that is roughly 50% smaller than the 2-D direct wave results, generally less than 0.15 for frequencies less than 2.0 Hz, similar to results in Turkey from Eken et al., (2004). Third, 2-D coda path corrections result in data scatter that is ~10% to 30% smaller than the 1-D coda results.

Although the coda amplitudes are corrected for frequency-dependent path effects, they still carry the *S*-to-coda transfer function as well as site effects and must be removed in order to obtain a moment-rate spectrum that has absolute units (*e.g.*, newton-meter). We note that the *S*-to-coda transfer function is likely not station dependent and is therefore assumed to be common to all events in this region. Practically speaking, however, we have no way of differentiating this effect from the station site effect. Therefore we simply lump $S(f)$ and $T(f)$ together and call it the "moment-rate" correction term. We used the moment calibration and empirical Green's function procedure outlined in Mayeda et al. (2003), which uses a handful of independently derived seismic moments to tie the low-frequency (*f*

< ~1.0 Hz) coda amplitudes to an absolute scale and smaller events as empirical Green's functions to derive corrections for the higher frequencies (f > ~1.0 Hz). In our case, we chose 10 events from the BSL's moment-tensor catalog with magnitudes ranging between M_W 3.6 to 5.5. Assuming that the smallest of our calibration events has a corner frequency around 1 Hz, we can find the frequency-dependent corrections that, in a least-squares sense, match our 10 independent moments, thereby giving us the corrections between $0.05 \leq f \leq 1.0$ Hz. For frequencies above 1 Hz we use small empirical Green's function events noting that the these events are around M_W ~2 to 2.5 based on their 1-Hz amplitudes, and we assume that on average, these small events have flat-source spectra of at least up to 8.0 Hz, the highest frequency that we are considering. The procedure to derive moment-rate corrections was done station-by-station. Using the average of the two lowest frequency values, we computed M_W from the coda-derived spectra. The same procedure was applied to the direct-wave amplitudes to correct for the site effect. We find excellent agreement between our coda-derived moment magnitudes and the BSL's. Figure 4a shows an example of 1-D, coda-derived source spectra for the M_W 5.3 Napa earthquake of September 3, 2000, and Figure 4b shows the corresponding *S*-wave source spectra using all 16 stations. (We note that the 2-D coda results exhibit a tighter distribution especially at frequencies above 2.0 Hz). Though more scattered, the average of the direct wave spectra is very similar to the individual coda spectra, thus proving the point that a single-station coda spectra is roughly equivalent to a 9-station average using direct waves. The stability of the coda-derived spectra is remarkable, considering that they are derived from different azimuths and distances, mixing local *S*-wave, regional L_g, and surface wave codas.

CONCLUSIONS

As a test of the two methods, we chosen over 140 well-located earthquakes ($3.5 < Mw < 6.5$) distributed throughout the northern California region recorded on high-quality broadband stations of the Berkeley Digital Seismic Network (BDSN). The complicated tectonics of the region coupled with these high-quality data, provides for an ideal situation to test the two approaches. We found that source spectra derived from the 2-D approach were essentially identical to those from the 1-D approach for frequencies less than ~0.7-Hz; however, for the high frequencies ($0.7 < f < 8.0$ Hz), the 2-D approach resulted in interstation scatter that was generally 30% smaller. Because our main objective is to improve moment-magnitude estimation for small regional events, the 30% improvement is significant in helping to meet the U.S.'s monitoring goals. Our findings are as follows: (1) 2-D path corrections for the direct waves significantly reduce the scatter over 1-D corrections; however, interstation scatter remains large, ranging between ~0.2 and 0.3 for $0.05 < f < 8.0$-Hz; (2) 1-D coda path corrections result in scatter that is roughly 50% smaller than the 2-D direct wave results; (3) 2-D coda path corrections result in data scatter that is ~10 to 30% smaller than the 1-D coda results.

REFERENCES

Aki, K. (1969), Analysis of Seismic Coda of Local Earthquakes as Scattered Waves, *J. Geophys. Res*., 74, 615-631.

Aki, K. and B. Chouet (1975), Origin of Coda Waves: Source, Attenuation and Scattering Effects, *J. Geophys. Res*. 80, 3322-3342.

Dreger, D. S. and D. V. Helmberger (1993), Determination of Source Parameters at Regional Distances with Single Station or Sparse Network Data, *J. Geophys. Res*. 98, 8107-8125.

Dreger, D. and B. Romanowicz (1994), Source Characteristics of Events in the San Francisco Bay Region, *USGS Open-file report, 94-176*, 301-309.

Dreger D. and B. Woods (2002), Regional Distance Seismic Moment Tensors of Nuclear Explosions, *Tectonophysics*, in press.

Dreger, D. S., D. Oglesby, R. Harris, N. Ratchkovski, and R. Hansen (2003), Kinematic and Dynamic Rupture Models of the November 3, 2002 *M*w7.9 Denali, Alaska Earthquake, submitted to *Geophys. Res. Lett*.

Eken, T., K. Mayeda, A. Hofstetter, R. Gök, G. Örgülü and N. Turkelli (2004), An Application of the Coda Methodology for Moment-rate Spectra Using Broadband Stations in Turkey, *Geophys. Res. Lett*. 31.

Fukuyama, E., M. Ishida, D. Dreger, and H. Kawai (1998), Automated Seismic Moment Tensor Determination by Using on-line Broadband Seismic Waveforms, *Jishin, 51*, 149-156.

Fukuyama, E. and D. Dreger (2000), Performance Test of an Automated Moment Tensor Determination System, *Earth Planets Space, 52*, 383-392.

Kaverina, A., D. Dreger, and E. Price (2002), The Combined Inversion of Seismic and Geodetic Data for the Source Process of the 16 October 1999 Mw 7.1 Hector Mine, California, Earthquake, *Bull. Seism. Soc. Am.* 92, 1266-1280.

Malagnini, L., K. Mayeda, A. Akinci, and P.L. Bragato (2004), Estimating Absolute Site Effects, *Bull. Seismol. Soc. Am*., in press.

Mayeda, K., A. Hofstetter J. L. O'Boyle, and W. R Walter (2003), Stable and Transportable Regional Magnitudes Based on Coda-derived Moment-rate Spectra. *Bull. Seismol. Soc. Am.,* 93, 224-239.

Mayeda, K. and W.R. Walter (1996), Moment, Energy, Stress Drop, and Source Spectra of Western United States Earthquakes from Regional Coda Envelopes. *J. Geophys. Res.* 101, 11, 195-11,208.

Morasca, P., L. Malagnini, A. Akinci, and D. Spallarossa (2004), Ground-motion Scaling in the Western Alps. *Bull. Seism. Soc. Am. (submitted)*.

Örgülü, G., and M. Aktar (2001), Regional Moment Tensor Inversion for Strong Aftershocks of the August 17, 1999 Izmit Earthquake (MW-7.4), *Geophys. Res. Lett*., 28, 371-374.

Pasyanos, M. E., D. S. Dreger, and B. Romanowicz (1996), Towards Real-Time Determination of Regional Moment Tensors, Bull. Seism. Soc. Am., 86, 1255-1269.

Rautian, T. G. and V. I. Khalturin (1978), The Use of the Coda for the Determination of the Earthquake Source Spectra, *Bull. Seism. Soc. Am*. 68, 923-948.

Romanowicz, B., M. Pasyanos, D. Dreger, and R. Uhrhammer (1993), Monitoring of Strain Release in Central and Northern California Using Broadband Data, *Geophys. Res. Lett. 20*, 1643-1646.

Sato, H. and Fehler (1998), M, Seismic Wave Propagation and Scattering in the Heterogeneous Earth. *AIP Press, Modern Acoustic and Signal Processing*.

Street, R. L., R. Herrmann, and O. Nuttli (1975), Spectral Characteristics of the Lg Wave Generated by Central United States Earthquakes, *Geophys. J. R. Astr. Soc.,* 41, 51-63.

Tajima, F., C. Mégnin, D. Dreger, and B. Romanowicz (2002), Feasibility of Real-time Broadband Waveform Inversion for Simultaneous Moment tensor and Centroid Location Determination, *BSSA, 92, 739-750*.

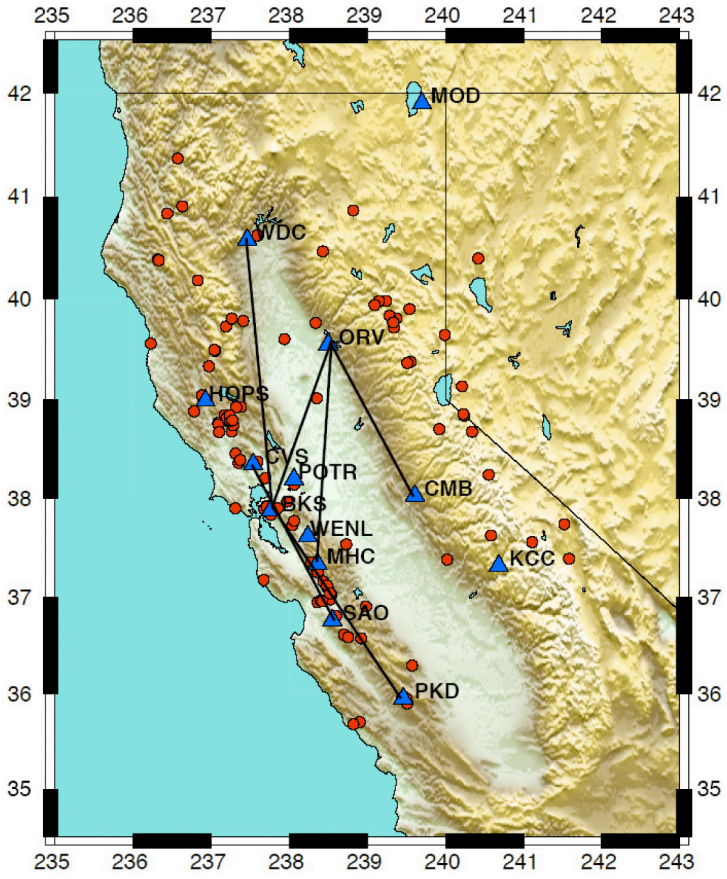

Figure 1 Map of events and stations used in this study. Lines show station pairs that were used in the 1-D coda and 1-D direct wave path corrections.

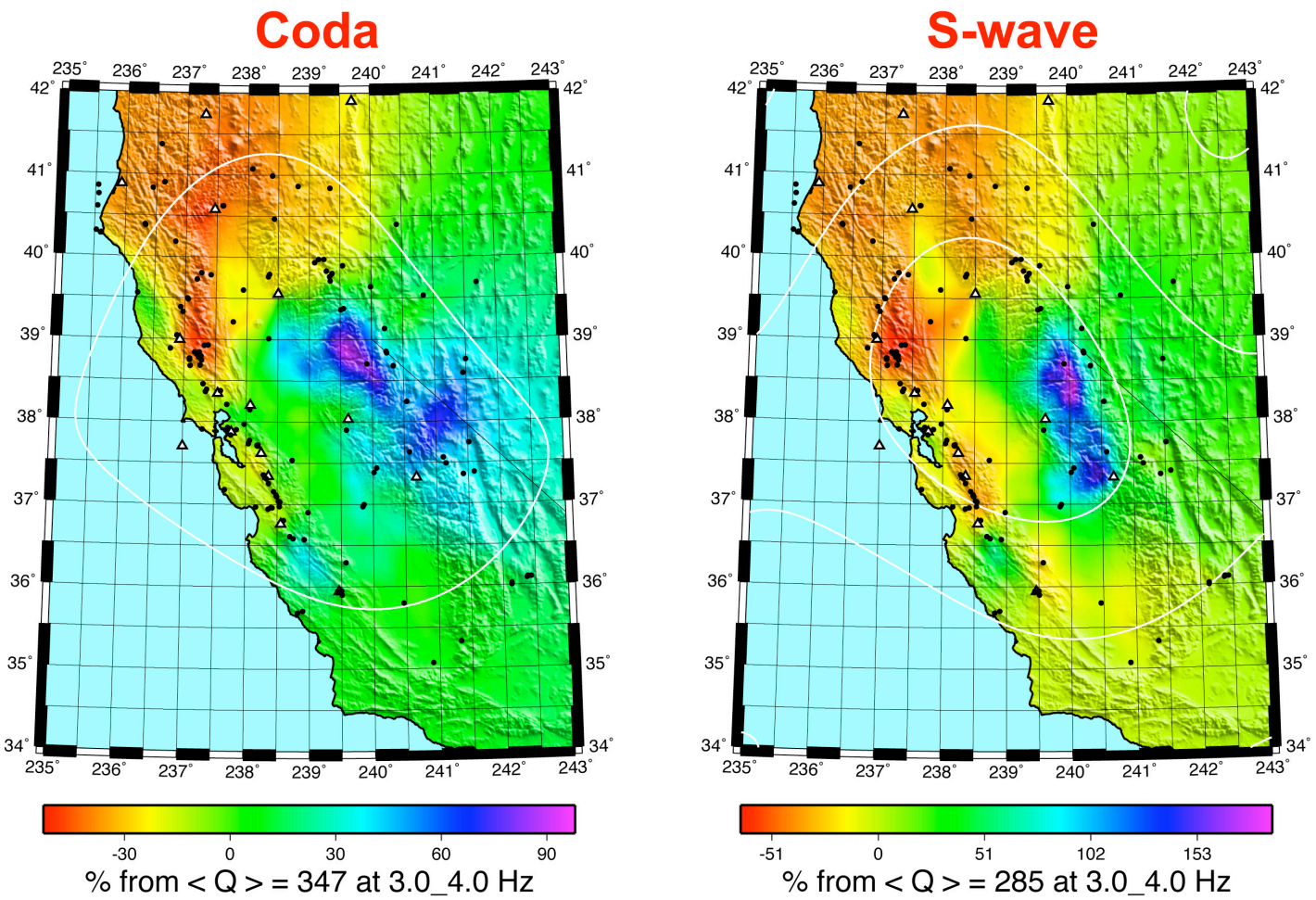

Figure 2 Maps of Q from coda wave and S-wave inversion using the same station and event distribution.

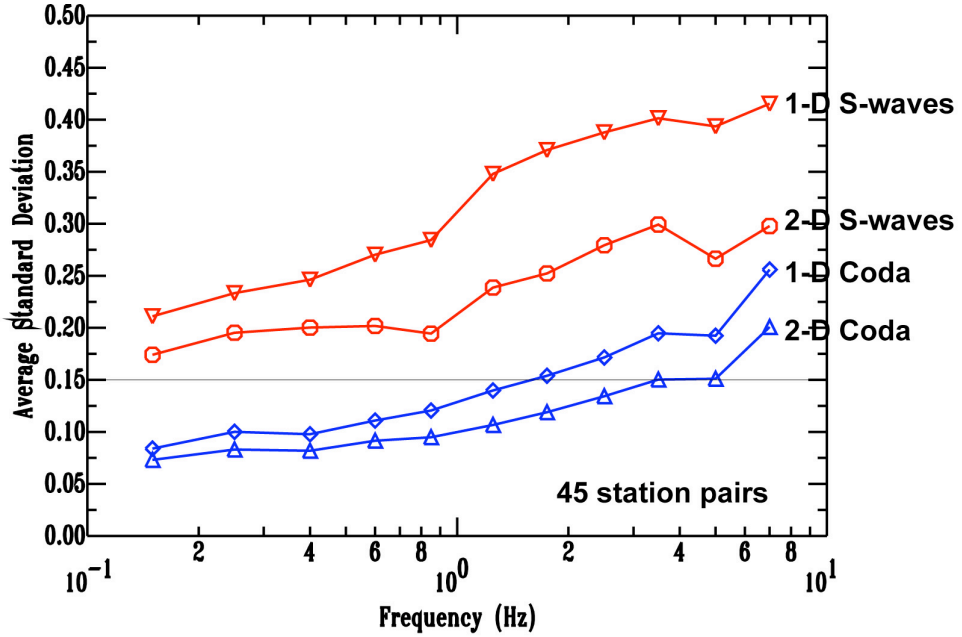

Figure 3 Average interstation data standard deviation for all four methods using the same events and stations. Notice that even the 1-D coda is far better than a 2-D inversion using direct waves. The 2-D coda allows for even more improvement by up to 30%.

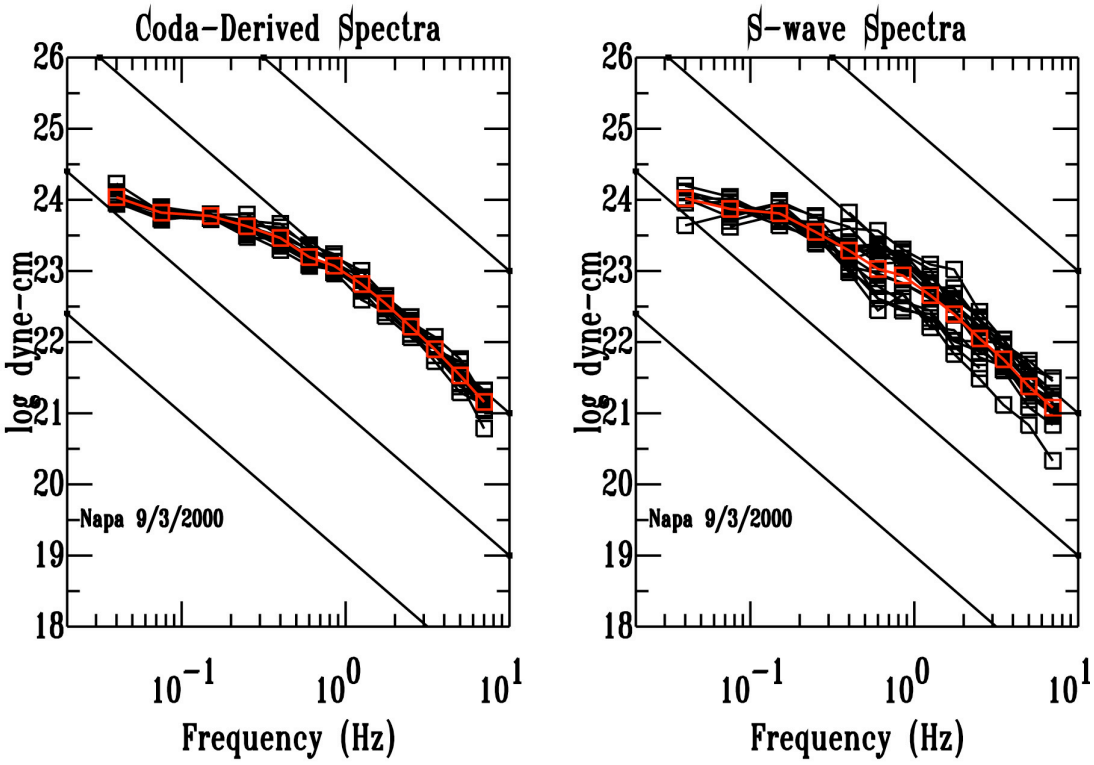

Figure 4 Moment-rate spectra for the September 3, 2000 Napa earthquake using 1-D coda and 1-D direct waves. Notice that a single coda-derived spectra is nearly equivalent to the average direct wave spectra.